ARTICLES SCIENCE CHINA Materials

mater.scichina.com link.springer.com

Published online 29 May 2018 | https://doi.org/10.1007/s40843-018-9291-y
Sci China Mater 2018, 61(12): 1614–1622

Chemical synthesis, structure and magnetic properties of Co nanorods decorated with Fe_3O_4 nanoparticles

Shuang Qiao[1], Ziyu Yang[1], Junjie Xu[1], Xiaobai Wang[1], Jinbo Yang[2] and Yanglong Hou[1*]

ABSTRACT **Magnetic anisotropic nanocomposites have attracted tremendous interests, due to their unexpected properties originating from the interactions of the interfaces except for the intrinsic features. In this work, we develop a facile solution chemistry synthesis method to prepare the one-dimensional (1D) Co-Fe_3O_4 heterostructures with hard magnetic property. Interestingly, the Fe precursor firstly decompose and nucleate individually, and then grow on the surface of the hexagonal closed-packed (hcp) Co nanorods (NRs) upon prolonging heating time at higher temperature, which is different from the general seed-mediated growth model. The distribution density of Fe_3O_4 nanoparticles (NPs) on the surface of the Co NRs can be varied with the addition of Fe source, modulating the values of coercivity and saturation magnetization for the Co-Fe_3O_4 heterostructures. The as-synthesized Co-Fe_3O_4 heterostructures maintain the hard magnetic properties with a coercivity value more than 2.5 kOe as well as a saturation magnetization value up to 128.3 emu g^{-1}, indicating the preservation of the anisotropy of the hcp Co NRs.**

Keywords: chemical synthesis, Co nanorods, Co-Fe_3O_4 heterostructures, magnetic property

INTRODUCTION

Magnetic heterostructured nanocomposites have been intensively explored in varied areas such as advanced motors, biomedicine and magnetic data storage [1–3], and researchers paid more attention to combine the advantages of several different components to synthesize such materials [4,5]. From the perspective of functionalization, the construction of heterostructured nanocomposites enhances the performed functionalities due to the contribution of the individual component and synergic effects, which favors the exploitation of novel platforms beyond each ingredient [6]. Regarding to the synthesis strategies, physical vapor deposition [7], chemical vapor deposition [8], self-assembly [9], solvothermal route [10,11] and electrochemical deposition [12] are widely developed to synthesize the heterostructured nanocomposites. Among all of these strategies, the solution chemistry synthesis is prominent in controlling the size, composition and morphology of the target materials, thus becoming a general method to prepare these materials. In the last few years, a variety of inorganic heterostructured nanocomposites have been synthesized by the solution chemistry route [13,14], such as FePt-Co (or Ni, Fe_2C, Au) nanoparticles [15,16], FePd-Fe_3O_4 urchin-like nanocomposites [17], Au/Ag-Fe_3O_4 dumbbell-like nanostructures [18], and metal-tipped semiconductor nanorods (NRs) [19,20], providing a new approach to develop diverse heterostructured nanocomposites with high performance as well as novel applications. More importantly, the one-dimensional (1D) heterostructures which contain a nanorod base decorated with a functional layer, cause great concern of the researchers [21,22], and these materials are ready for manufactured devices and ideal building blocks in varied applications [23–26].

Ferromagnetic Co NRs with their long axis parallel to the hexagonal closed-packed (hcp) *c* axis exhibit excellent shape and magneto-crystalline anisotropy, and they also possess quite high coercivity (H_c) and saturation magnetization (M_s) values [27]. Owing to their distinct mechanical, electronic and magnetic properties [28,29], the Co NRs have great potential applications in the fields of high-density data storage devices [30] and permanent magnetic materials [31]. Several methods have been ap-

[1] Beijing Key Laboratory for Magnetoelectric Materials and Device (BKLMMD), Beijing Innovation Center for Engineering Science and Advanced Technology (BIC-ESAT), Department of Materials Science and Engineering, College of Engineering, Peking University, Beijing 100871, China
[2] State Key Laboratory for Mesoscopic Physics, School of Physics, Peking University, Beijing 100871, China
* Corresponding author (email: hou@pku.edu.cn)

plied to synthesize the anisotropic Co NRs, including electrochemical deposition [32], thermal decomposition of organometallic precursors ([Co(η^3-C_8H_{13})(η^4-C_8H_{12})] [33] or [Co{N($SiMe_3$)$_2$}$_2$] [34]) in a mixture of a long-chain acid and an amine as stabilizing agent, solvothermal process [35] and so on. In addition, the hcp Co NRs have been used for fabricating multiple heterostructures based on their high magnetic anisotropy and high saturation magnetization values, such as Co-CoSb core-shell NRs [36], Co-SnAu/SnPt core-shell NRs [37], Co-Au hybrid NRs [38] and Co-Fe nanodumbbells [39]. However, there are several remaining challenges in the synthesis of the Co NRs based heterostructured nanocomposites with desired component and morphology. For the sake of the high coercivity in these materials, the morphology of the Co NRs should not be altered by the introduction of the other component. Meanwhile, the ratio of the Co NRs to the other material must be modulated elaborately and the key point is to control the heterogrowth of the second component on the Co NRs. Besides, whether the second part can grow epitaxially on the surface of the Co NRs depends on the lattice mismatch between the Co NRs and alternative second ingredient.

Herein, we synthesized the one-dimensional (1D) Co-Fe_3O_4 heterostructures by growing Fe_3O_4 nanoparticles (NPs) on the surface of the pre-prepared Co NRs without altering the hcp structure of the Co NRs. From the characterization results, it can be concluded that the higher temperature process enables the epitaxial growth of the Fe_3O_4 NPs on the surface of the Co NRs and the ratio of Fe/Co can be tuned by controlling the concentration of $Fe(CO)_5$ in the liquid phase reaction system. Besides, the magnetic characterization demonstrates that the as-synthesized Co-Fe_3O_4 heterostructures maintain hard magnetic properties, indicating the preservation of the anisotropy of the hcp Co NRs. Moreover, the facile chemical method reported in our study can be extended to prepare other heterostructured nanocomposites.

EXPERIMENTAL SECTION

Chemicals

All the raw chemicals were used without additional purification. Cobalt (II) chloride hexahydrate ($CoCl_2{\cdot}6H_2O$, 99.9%), 1-octadecene (ODE, tech. 90%) and 1-hexadecylamine (HAD, tech. 90%, remainder mainly 1-octadecylamine) were purchased from Alfa Aesar. Ruthenium chloride ($RuCl_3$, Aldrich, 45%–55% Ru content), oleylamine (OAm, tech. 70 %), oleic acid (OA, 99%) and lauric acid ($C_{11}H_{23}COOH$, 98%) were bought from Sigma Aldrich. NH_4Br (99%) was purchased from J&K Chemicals. Sodium hydroxide (NaOH, AR) was bought from Xilong Chemical Co., Ltd, Guangdong, China. 1,2-Butanediol (98%) was purchased from Tokyo Chemical Industry Co. Ltd and iron pentacarbonyl ($Fe(CO)_5$) was got from Tianyi Co. Ltd, Jiangsu, China.

Synthesis of Co NRs

The starting Co NRs were synthesized by the solvothermal process according to a previous method [27]. Firstly, cobalt (II) laurate ($Co(C_{11}H_{23}COO)_2$) was prepared by mixing 44.0 mmol of lauric acid and 42.0 mmol of NaOH with 40 mL of deionized water using a mechanical stirrer. The mixture was heated to 60°C until a clear solution was obtained and then 10 mL of an aqueous solution of 2 mol L^{-1} $CoCl_2{\cdot}6H_2O$ was added dropwise to the clear solution. Finally, the obtained purple precipitate was washed with deionized water for several times and dried overnight at 60°C to remove the excess water.

The Co NRs were synthesized by the reduction of cobalt (II) laurate in a basic solution of 1,2-butanediol. Firstly, cobalt (II) laurate (2.29 g), $RuCl_3$ (0.026 g), HAD (0.644 g), NaOH (48.0 mg) and 60 mL of 1,2-butanediol were introduced into a teflon enclosure (100 mL). Afterwards, the teflon enclosure was purged with inert gas (N_2) for 30 min before sealed, and then fitted within an autoclave reactor. Subsequently, the autoclave reactor was transferred to a furnace and heated from room temperature to 200°C and maintained at that temperature for 90 min. After cooled down to room temperature, the products were collected by centrifugation and redispersed in hexane (10 mL).

Synthesis of Co-Fe_3O_4 heterostructures

The Co-Fe_3O_4 heterostructures were synthesized by adding iron precursor ($Fe(CO)_5$) to the solution of the pre-prepared Co NRs [40]. In a typical process, 1.0 mmol of Co NRs in ODE (20 mL), OAm (2.0 mL), OA (0.5 mL) and 3.5 mg of NH_4Br were mixed in a four-neck flask and degassed under forming gas (Ar 95%+H_2 5%) at 120°C for at least 30 min. After that, the temperature was increased to 180°C and a certain amount of $Fe(CO)_5$ was injected rapidly into the mixed solution, and then kept at 180°C for additional 30 min. Afterwards, the temperature was increased to 250°C at a rate of 5°C min^{-1} and kept at that temperature for another 15 min. The products were purified by precipitation in ethanol, followed by redispersing in hexane and precipitating out by adding ethanol for several times. Finally, the purified products were redispersed in hexane (10 mL).

In all experiments, the concentration of the Co NRs, solvent and surfactants kept constant, and the reaction condition was not changed. Three targeted samples with different Fe/Co compositions were synthesized by varying the concentration of $Fe(CO)_5$. To get the targeted sample, 20, 50 and 80 μL of $Fe(CO)_5$ was added to the reaction system contained 1.0 mmol of Co NRs, respectively, and the obtained samples were consequently named as Co-Fe_3O_4-20, Co-Fe_3O_4-50 and Co-Fe_3O_4-80.

Characterizations

The morphological characterization of the products was carried out by a FEI Tecnai T20 transmission electron microscope (TEM) at 200 kV, and the high resolution TEM (HRTEM) images and EDS chemical mapping were obtained on a Tecnai-G2-F30 (FEI) transmission electron microscope at an acceleration voltage of 300 kV. Samples for TEM analyses were prepared by drying the dispersion of the samples on amorphous carbon coated Cu grids. Scanning electron microscopy (SEM) characterization was done using a Hitachi S-4800. X-ray diffraction (XRD) patterns were obtained by using a PANalytical X'Pert^3 Powder X-ray diffractometer equipped with Cu-Kα radiation, with the accelerating voltage and current of 40 kV and 40 mA, respectively and the XRD patterns were performed in the 2θ range of 25–85°. X-ray photoelectron spectroscopy (XPS) patterns were collected on Imaging Photoelectron Spectrometer (Axis Ultra DLD, Kratos Analytical Ltd.) by using monochromatized Al Kα anode ($h\nu$=1,486.7 eV), and the pressures in the analysis chamber was 10^{-8}–10^{-9} torr. The magnetic properties of the powders of randomly oriented Co NRs and Co-Fe_3O_4 heterostructures were investigated up to 3T *via* a Physical Property Measurement System (DynaCool, Quantum Design) at room temperature. All of the samples were purified and sealed in plastic capsules before characterization and the absolute magnetization value was deduced from the content of Co, or Co and Fe_3O_4 determined by inductively coupled plasma atomic emission spectroscopy (ICP-AES).

RESULTS AND DISCUSSION

By using a facile solvothermal chemical process, we prepared well-distributed hcp Co NRs. SEM and TEM images (Fig. 1a, b) show that the obtained Co NRs possess cylinder shapes with ellipsoidal tips and disperse homogeneously. More SEM images of the Co NRs are shown in Fig. S1a, b, and the statistical data in Fig. S1e reveal that the Co NRs have a mean size of 150–200 nm in length and an average diameter of about 15 nm. In addition, the

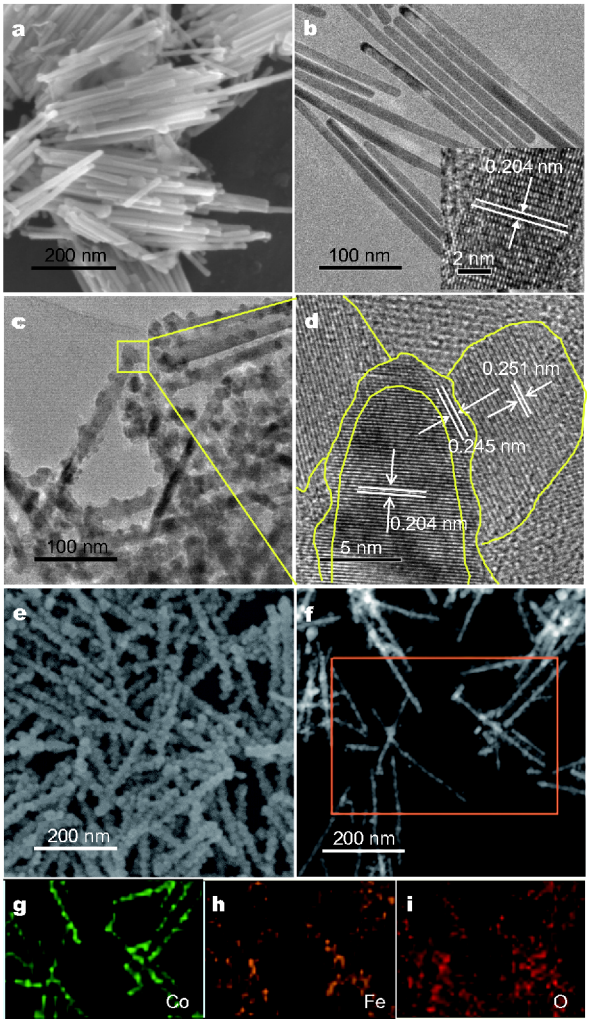

Figure 1 (a) SEM image, (b) TEM and HRTEM image (insert) of the Co NRs. (c, d) TEM and HRTEM images of the Co-Fe_3O_4 heterostructures, (e) SEM image. (f–i) EDS chemical mapping of the Co-Fe_3O_4 heterostructures, showing the distribution for the elements of Co, Fe and O (Co: green, Fe: orange and O: red).

insert HRTEM image in Fig. 1b displays a lattice fringe of 0.204 nm, corresponding to hcp Co (002) facet [27], and the crystal structure of the as-synthesized Co NRs is also confirmed by XRD patterns (Fig. S2).

TEM image in Fig. 1c shows that the thermal decomposition of $Fe(CO)_5$ produced Fe_3O_4 NPs decorating on the surface of the Co NRs, forming the Co-Fe_3O_4 heterostructures. Fig. 1d is the HRTEM image representing one typical part of the Co-Fe_3O_4 heterostructure, which indicates the presence of a structure with nanoparticles surrounding the nanorod and it could be clearly seen that the Fe_3O_4 NPs decorate the tips and the whole body of the hcp Co NRs. Furthermore, the lattice fringes are exposed in both regions, and the fringes of 0.204 and 0.251 nm are

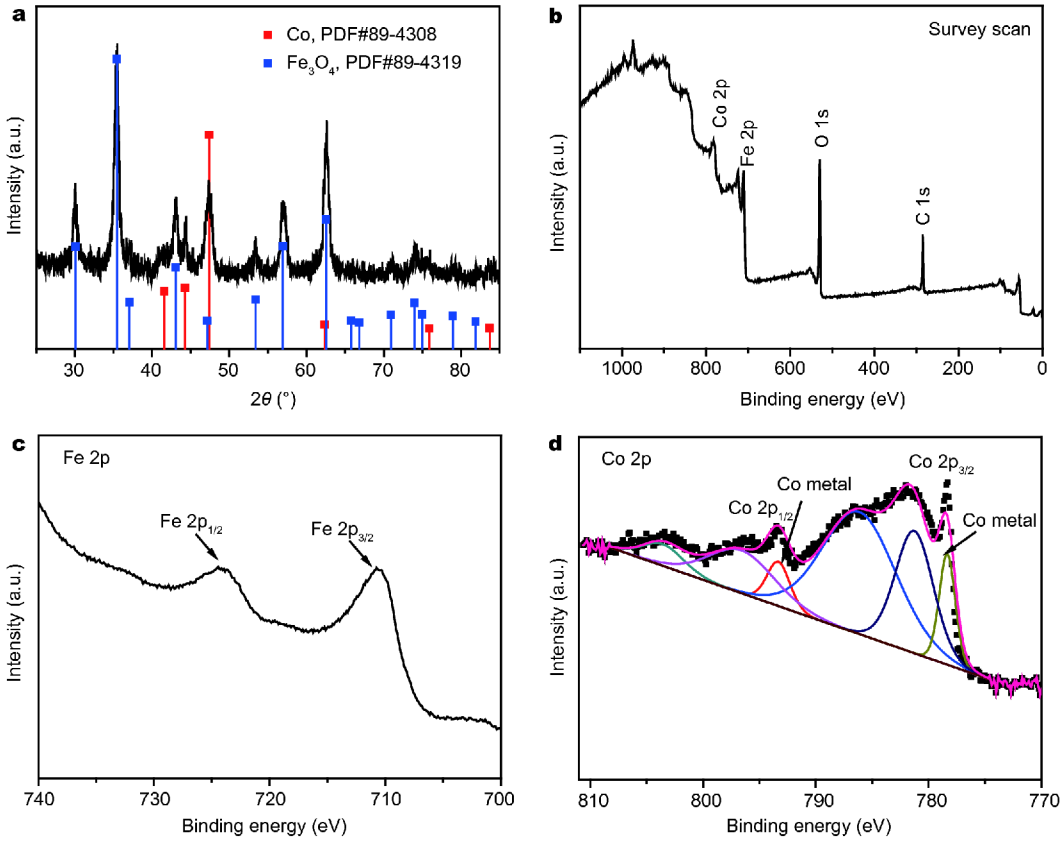

Figure 2 (a) XRD patterns and (b–d) survey and fitted XPS of the Co-Fe_3O_4 heterostructures. (b) Survey scan, (c) Fe 2p region and (d) Co 2p region.

observed in the inside nanorod and outer nanoparticle, corresponding to the lattice spacing of the Co (002) facet [27] and the Fe_3O_4 (311) facet [40], separately. Besides, it is worth noting that there is a transition layer between the nanorod and the nanoparticle structure, and the fringe of the layer is 0.245 nm, which is in accordance with the lattice spacing of (111) facet for CoO [41,42], suggesting that the fresh surface of the Co NRs is prone to be oxidized during the reaction firstly and then the Fe_3O_4 NPs will grow on the Co NRs. The SEM image in Fig. 1e shows the morphology of the Co-Fe_3O_4 heterostructures with uniform size and more SEM and TEM images are shown in Fig. S3. In order to detect the elements distribution within the heterostructures, EDS chemical mapping was performed, as presented in Fig. 1f–i, which clearly display that the Co content is located in the centre of the heterostructure and the Fe and O contents are located in the outer space.

The crystal structure of the sample is confirmed by XRD analysis (Fig. 2a), typical peaks of the Co and Fe_3O_4 can be observed, confirming the components of Co and Fe_3O_4 in the heterostructures. As a surface analysis technique, XPS was used to investigate the elements present at the surface as well as their chemical states. In our research, the XPS analysis was calibrated by the adventitious C 1s peak with a fixed value of 284.8 eV. Fig. 2b shows the overall survey spectrum of the as-synthesized Co-Fe_3O_4 heterostructures with scan binding energy (BE) from 0 to 1,100 eV, which reveals the presence of the Fe 2p, Co 2p, C 1s and O 1s peaks at their respective binding energy regions. The peak positions which locate at 710.6 and 724.1 eV are for Fe $2p_{3/2}$ and Fe$2p_{1/2}$ of Fe_3O_4, as shown in Fig. 2c, confirming the existence of Fe_3O_4 in the heterostructures [43]. In order to detect the existence of cobalt oxide in the samples, we have analysed the Co 2p regions. As shown in Fig. 2d, the characteristic peaks at about 778.5 and 793.4 eV, correspond to metallic Co $2p_{3/2}$ and Co $2p_{1/2}$, separately [44,45], which confirms the metallic Co in the heterostructures. In addition, the BE values of 780.5 and 796.5 eV correspond to the Co $2p_{3/2}$ and Co $2p_{1/2}$ for monoxide, respectively [42,46], and the apparent satellites clearly indicate the existence of Co (II) [47–49], further confirming the existence of cobalt oxide in the Co-Fe_3O_4 heterostructures.

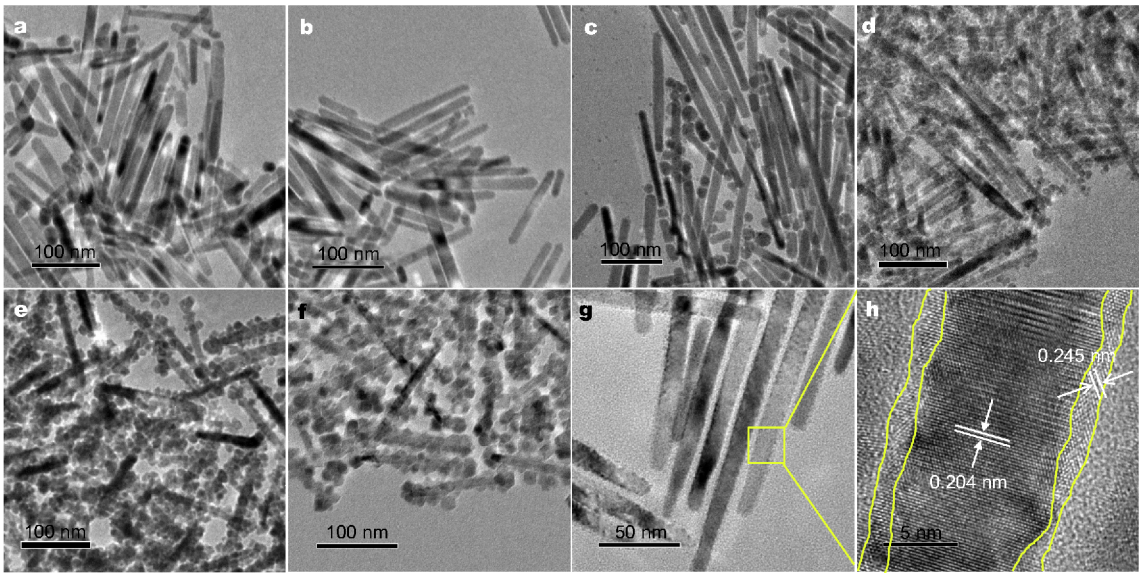

Figure 3 (a–f) TEM images of the samples obtained under different reaction stage: (a) 180°C for 15 min, (b) 180°C for 30 min, (c) 250°C for 0 min, (d) 250°C for 5 min, (e) 250°C for 10 min and (f) 250°C for 15 min. (g, h) TEM and HRTEM images of the sample obtained without the addition of $Fe(CO)_5$.

The formation mechanism of Co-Fe_3O_4 heterostructures

To investigate the formation mechanism of the Co-Fe_3O_4 heterostructures, we characterized the products in multi-stage reaction process by TEM. At the first stage, when an appropriate amount of $Fe(CO)_5$ was added into the reaction system at 180°C, there was no obvious change for the Co NRs, as shown in Fig. 3a, b. According to the classic theory of crystal growth, the materials tend to nucleate individually due to the supersaturation under the thermodynamic environment. This temperature enables the thermal decomposition and nucleation of Fe precursor, but there are no particles decorated on the surface of the Co NRs directly, due to the large mismatch of the lattice constant between the two ingredients. When the temperature just increases to 250°C, there is still no apparent change for the Co NRs (Fig. 3c). However, further extending the reaction time, it can be found that the particles are inclined to gather along the Co NRs, as seen in Fig. 3d, and the higher temperature leads to the growth of Fe_3O_4 NPs on the surface of the Co NRs (Fig. 3e, f). The reason is that the crystal nuclei of Fe_3O_4 tend to grow on the surface of the defected Co NRs during the continuous growth with much less energy barriers. The XRD patterns of these products are shown in Fig. S4a. In order to clearly investigate what might happen to the Co NRs during the reaction, we synthesized the sample without adding Fe source under the same condition. Fig. 3g, h show the TEM and HRTEM images of this sample, where the fringes of 0.204 and 0.245 nm in the nanorod and outer layer correspond to the Co (002) facet [27] and CoO (111) facet [41,42], respectively. Thus, there is actually a layer of cobalt oxide whose thickness is 1–2 nm on the surface of the Co nanorod and it can be concluded that the high temperature process at 250°C may contribute to the oxidization of the surface of the Co NRs so that the Fe_3O_4 NPs can coat on the surface of Co NRs. The above results indicate that the growth of the Co-Fe_3O_4 heterostructures experiences a process including (Scheme 1): firstly, the thermal decomposition of $Fe(CO)_5$ and the oxidization of the surface of the Co NRs, and subsequently, the decoration of Fe_3O_4 NPs on the surface of the Co NRs. This may be due to the fact that the mismatch value between the crystal lattice of Co and Fe_3O_4 is much larger, so it is difficult for Fe_3O_4 NPs to decorate on the surface of the Co NRs directly. Therefore, in the first stage, the surface of the Co NRs is oxidized and a layer of cobalt oxide is formed. Since the mismatch value between the cobalt oxide and Fe_3O_4 allows the epitaxial growth of Fe_3O_4 NPs, the Fe_3O_4 NPs can grow and crystallize on the surface of the Co NRs. Based on this, it is assumed that because of the existence of cobalt oxide layer outside the Co NRs, the Fe_3O_4 NPs can decorate onto them.

According to the above results, we can deduce the reason why the layer of cobalt oxide generates on the surface of the Co NRs, and a possible explanation is that

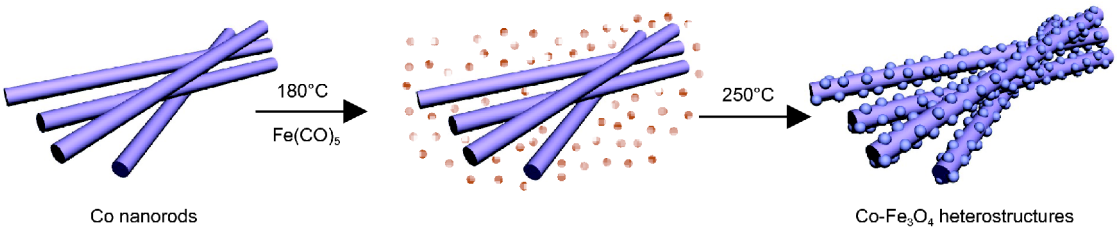

Scheme 1 The formation scheme of the Co-Fe_3O_4 heterostructures.

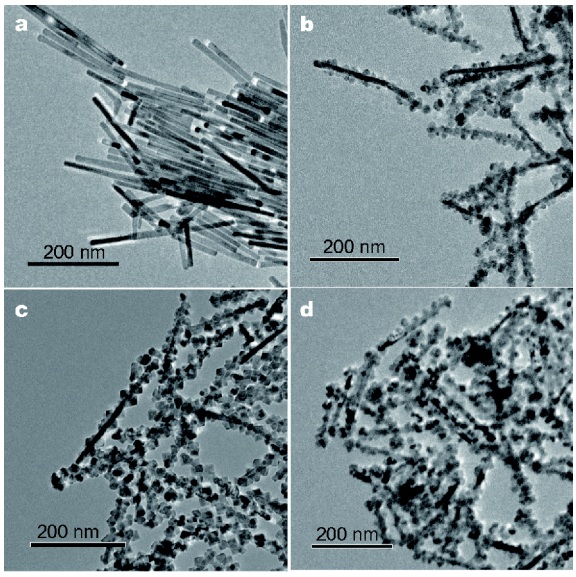

Figure 4 TEM images of the (a) Co NRs, (b) Co-Fe_3O_4-20, (c) Co-Fe_3O_4-50, (d) Co-Fe_3O_4-80.

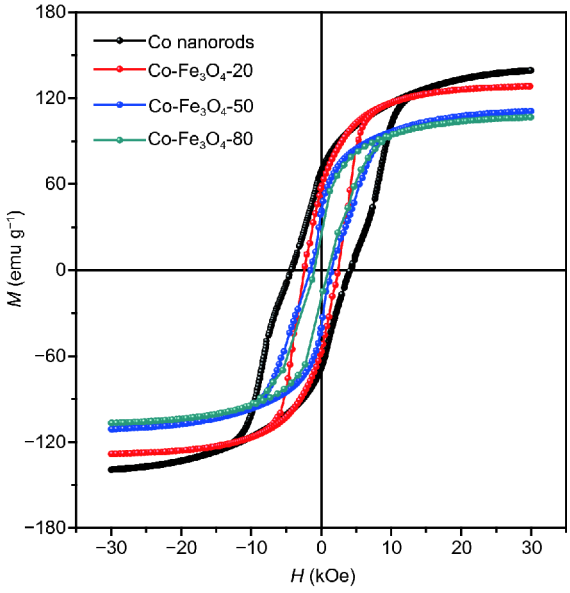

Figure 5 *M-H* loops of the Co-Fe_3O_4 heterostructures.

in the reaction system of ODE, OA and OAm, the surface of the as-prepared Co NRs can be oxidized very easily. By altering the surfactants in the reaction system, it is revealed that OA plays an important role in the formation process of the Co-Fe_3O_4 heterostructures (Fig. S5), which may be due to the oxidation effect of OA on the surface of the Co NRs, thus the surface of the Co NRs can be oxidized and then the Fe_3O_4 NPs could decorate onto them.

The effect of the Fe/Co ratio

The TEM images of the samples with different Fe/Co ratios are shown in Fig. 4. When the amount of $Fe(CO)_5$ is 20 μL, the amount of Fe_3O_4 NPs decorated on the surface of the Co NRs is less, and there is still some naked area remaining on the Co NRs. As the Fe/Co ratio increases, completely covered Co NRs by Fe_3O_4 NPs are obtained, and the decoration density of Fe_3O_4 on the surface of the Co NRs becomes more intensive. In addition, the XRD patterns indicate that the nanostructures are the mixture of hcp Co and Fe_3O_4 (Fig. S4b).

Magnetic properties of Co-Fe_3O_4 heterostructures

The magnetization measurement for pure Co NRs and the Co-Fe_3O_4 heterostructures of different Fe_3O_4 content were characterized *via M-H* loops with an applied magnetic field up to 3 T at room temperature, as shown in Fig. 5. Just as expected, both the initial Co NRs and the Co-Fe_3O_4 heterostructures exhibit ferromagnetic behavior at room temperature. Specifically speaking, the initial Co NRs display a M_s value of 142.2 emu g^{-1} and a high H_c value of about 4.2 kOe, resulting from their high shape and magneto-crystalline anisotropy. When the magnetic field is around zero, there is a kink, possibly because of the magnetostatic interaction between the magnetic materials [50,51]. Besides, it can be concluded that both the values of H_c and M_s for the Co-Fe_3O_4 heterostructures change with the various amount of Fe_3O_4, and they still retain hard magnetic properties, indicating the preserva-

tion of the anisotropy of the hcp Co NRs. Among all of the Co-Fe_3O_4 heterostructures, the Co-Fe_3O_4-20 presents the highest M_s value of 128.3 emu g^{-1} and keeps a H_c value which is more than 2.5 kOe. Fig. S6 shows the *M-H* loop for the Co-Fe_3O_4-20 at 4 K and its zero-field-cooling (ZFC) and field-cooling (FC) curves. There is an apparent kink in the *M-H* loop at 4 K where the magnetic field is near zero, indicating the two phases in the Co-Fe_3O_4 heterostructures (Fig. S6a). Typical ferromagnetic behavior is observed for the sample from the FC-ZFC curves, with no typical blocking temperature of T_b due to the presence of ferromagnetic Co NRs (Fig. S6b).

CONCLUSIONS

In this work, we investigated the chemical synthesis, structure and magnetic properties of the Co-Fe_3O_4 heterostructures, which were obtained by decorating Co NRs with Fe_3O_4 NPs. The Co-Fe_3O_4 heterostructures with different decoration density of Fe_3O_4 NPs can be synthesized upon tuning the amount of Fe source in the reaction solution. Furthermore, it can be concluded that the epitaxial growth of the Fe_3O_4 NPs on the surface of the Co NRs experiences a process of the thermal decomposition of $Fe(CO)_5$ and the oxidization of the surface of Co NRs, and subsequently the decoration of Fe_3O_4 NPs on the surface of the Co NRs, differing from the general seed-mediated growth model. More importantly, the magnetic measurements indicate that the integrity of the anisotropic Co NRs is preserved after the epitaxial growth of Fe_3O_4 NPs, for the whole structure still retain hard magnetic properties with a H_c value higher than 2.5 kOe and a M_s value of 128.3 emu g^{-1}. The chemical synthesis strategy reported in our work can be applied to the synthesis of other nanocomposites.

Received 21 March 2018; accepted 28 April 2018; published online 29 May 2018

1 Song Q, Zhang ZJ. Controlled synthesis and magnetic properties of bimagnetic spinel ferrite $CoFe_2O_4$ and $MnFe_2O_4$ nanocrystals with core–shell architecture. J Am Chem Soc, 2012, 134: 10182–10190
2 Ju Y, Zhang H, Yu J, *et al.* Monodisperse Au–Fe_2C Janus nanoparticles: an attractive multifunctional material for triple-modal imaging-guided tumor photothermal therapy. ACS Nano, 2017, 11: 9239–9248
3 Lu Y, Shi C, Hu MJ, *et al.* Magnetic alloy nanorings loaded with gold nanoparticles: synthesis and applications as multimodal imaging contrast agents. Adv Funct Mater, 2010, 20: 3701–3706
4 Salazar-Alvarez G, Lidbaum H, López-Ortega A, *et al.* Two-, three-, and four-component magnetic multilayer onion nanoparticles based on iron oxides and manganese oxides. J Am Chem Soc, 2011, 133: 16738–16741
5 Hao R, Xing R, Xu Z, *et al.* Synthesis, functionalization, and biomedical applications of multifunctional magnetic nanoparticles. Adv Mater, 2010, 22: 2729–2742
6 Liu F, Hou Y, Gao S. Exchange-coupled nanocomposites: chemical synthesis, characterization and applications. Chem Soc Rev, 2014, 43: 8098–8113
7 Hong L, Vilar RM, Youming W. Laser beam processing of a SiC particulate reinforced 6061 aluminium metal matrix composite. J Mater Sci, 1997, 32: 5545–5550
8 Kim YL, Jung JH, Yoon HS, *et al.* CdS/CdSe lateral heterostructure nanobelts by a two-step physical vapor transport method. Nanotechnology, 2010, 21: 145602
9 Xiao FX, Miao J, Liu B. Self-assembly of aligned rutile@anatase TiO_2 nanorod@CdS quantum dots ternary core–shell heterostructure: cascade electron transfer by interfacial design. Mater Horiz, 2014, 1: 259–263
10 Datt G, Sen Bishwas M, Manivel Raja M, *et al.* Observation of magnetic anomalies in one-step solvothermally synthesized nickel–cobalt ferrite nanoparticles. Nanoscale, 2016, 8: 5200–5213
11 Song J, Xiang J, Mu C, *et al.* Facile synthesis and excellent electrochemical performance of CoP nanowire on carbon cloth as bifunctional electrode for hydrogen evolution reaction and supercapacitor. Sci China Mater, 2017, 60: 1179–1186
12 Pan H, Liu B, Yi J, *et al.* Growth of single-crystalline Ni and Co nanowires *via* electrochemical deposition and their magnetic properties. J Phys Chem B, 2005, 109: 3094–3098
13 Yang Z, Zhao T, Huang X, *et al.* Modulating the phases of iron carbide nanoparticles: from a perspective of interfering with the carbon penetration of Fe@Fe_3O_4 by selectively adsorbed halide ions. Chem Sci, 2017, 8: 473–481
14 Hou Y, Sellmyer DJ. Magnetic Nanomaterials: Fundamentals, Synthesis and Applications. New York: John Wiley & Sons, 2017:
15 Wu J, Hou Y, Gao S. Controlled synthesis and multifunctional properties of FePt-Au heterostructures. Nano Res, 2011, 4: 836–848
16 Liu F, Zhu J, Yang W, *et al.* Building nanocomposite magnets by coating a hard magnetic core with a soft magnetic shell. Angew Chem Int Ed, 2014, 53: 2176–2180
17 Yu Y, Sun K, Tian Y, *et al.* One-pot synthesis of urchin-like FePd–Fe_3O_4 and their conversion into exchange-coupled $L1_0$–FePd–Fe nanocomposite magnets. Nano Lett, 2013, 13: 4975–4979
18 Wang C, Xu C, Zeng H, *et al.* Recent Progress in Syntheses and Applications of Dumbbell-like Nanoparticles. Adv Mater, 2009, 21: 3045–3052
19 Tian Y, Wang L, Yu S, *et al.* Heterostructure of Au nanocluster tipping on a ZnS quantum rod: controlled synthesis and novel luminescence. Nanotechnology, 2015, 26: 325702
20 Mokari T, Rothenberg E, Popov I, *et al.* Selective growth of metal tips onto semiconductor quantum rods and tetrapods. Science, 2004, 304: 1787–1790
21 Schrittwieser S, Ludwig F, Dieckhoff J, *et al.* Modeling and development of a biosensor based on optical relaxation measurements of hybrid nanoparticles. ACS Nano, 2012, 6: 791–801
22 Li A, Zou J, Han X. Growth of III-V semiconductor nanowires and their heterostructures. Sci China Mater, 2016, 59: 51–91
23 Li Y, Zhao J, You W, *et al.* Gold nanorod@iron oxide core–shell heterostructures: synthesis, characterization, and photocatalytic performance. Nanoscale, 2017, 9: 3925–3933
24 Ivanov YP, Chuvilin A, Lopatin S, *et al.* Modulated magnetic nanowires for controlling domain wall motion: toward 3D magnetic memories. ACS Nano, 2016, 10: 5326–5332

25 Lu Y, Xu YJ, Zhang G, *et al.* Iron oxide nanoclusters for T1 magnetic resonance imaging of non-human primates. Nat Biomed Eng, 2017, 1: 637–643
26 Lu Y, Dong L, Zhang LC, *et al.* Biogenic and biomimetic magnetic nanosized assemblies. Nano Today, 2012, 7: 297–315
27 Gandha K, Elkins K, Poudyal N, *et al.* High energy product developed from cobalt nanowires. Sci Rep, 2015, 4: 5345
28 Fang W, Panagiotopoulos I, Ott F, *et al.* Optimization of the magnetic properties of aligned Co nanowires/polymer composites for the fabrication of permanent magnets. J Nanopart Res, 2014, 16: 1–10
29 Ait Atmane K, Zighem F, Soumare Y, *et al.* High temperature structural and magnetic properties of cobalt nanorods. J Solid State Chem, 2013, 197: 297–303
30 Singamaneni S, Bliznyuk VN, Binek C, *et al.* Magnetic nanoparticles: recent advances in synthesis, self-assembly and applications. J Mater Chem, 2011, 21: 16819–16845
31 Maurer T, Ott F, Chaboussant G, *et al.* Magnetic nanowires as permanent magnet materials. Appl Phys Lett, 2007, 91: 172501
32 Cattaneo L, Franz S, Albertini F, *et al.* Electrodeposition of hexagonal Co nanowires with large magnetocrystalline anisotropy. Electrochim Acta, 2012, 85: 57–65
33 Dumestre F, Chaudret B, Amiens C, *et al.* Unprecedented crystalline super-lattices of monodisperse cobalt nanorods. Angew Chem Int Ed, 2003, 42: 5213–5216
34 Wetz F, Soulantica K, Respaud M, *et al.* Synthesis and magnetic properties of Co nanorod superlattices. Mater Sci Eng-C, 2007, 27: 1162–1166
35 Soumare Y, Garcia C, Maurer T, *et al.* Kinetically controlled synthesis of hexagonally close-packed cobalt nanorods with high magnetic coercivity. Adv Funct Mater, 2009, 19: 1971–1977
36 Sanyal U, Ener S, Anagnostopoulou E, *et al.* Co@CoSb core–shell nanorods: from chemical coating at the nanoscale to macroscopic consolidation. Chem Mater, 2016, 28: 4982–4990
37 Lentijo-Mozo S, Tan RP, Garcia-Marcelot C, *et al.* Air- and water-resistant noble metal coated ferromagnetic cobalt nanorods. ACS Nano, 2015, 9: 2792–2804
38 Wetz F, Soulantica K, Falqui A, *et al.* Hybrid Co–Au nanorods: controlling au nucleation and location. Angew Chem Int Ed, 2007, 46: 7079–7081
39 Liakakos N, Gatel C, Blon T, *et al.* Co–Fe nanodumbbells: synthesis, structure, and magnetic properties. Nano Lett, 2014, 14: 2747–2754
40 Knappett BR, Abdulkin P, Ringe E, *et al.* Characterisation of Co@Fe_3O_4 core@shell nanoparticles using advanced electron microscopy. Nanoscale, 2013, 5: 5765–5772
41 Maurer T, Zighem F, Ott F, *et al.* Exchange bias in Co/CoO core-shell nanowires: Role of antiferromagnetic superparamagnetic fluctuations. Phys Rev B, 2009, 80: 064427
42 Yang H, Ouyang J, Tang A. Single step synthesis of high-purity CoO nanocrystals. J Phys Chem B, 2007, 111: 8006–8013
43 Yamashita T, Hayes P. Analysis of XPS spectra of Fe^{2+} and Fe^{3+} ions in oxide materials. Appl Surf Sci, 2008, 254: 2441–2449
44 Biesinger MC, Payne BP, Grosvenor AP, *et al.* Resolving surface chemical states in XPS analysis of first row transition metals, oxides and hydroxides: Cr, Mn, Fe, Co and Ni. Appl Surf Sci, 2011, 257: 2717–2730
45 Liu B, Jin L, Zheng H, *et al.* Ultrafine Co-based nanoparticle@-mesoporous carbon nanospheres toward high-performance supercapacitors. ACS Appl Mater Interfaces, 2017, 9: 1746–1758
46 Langell MA, Anderson MD, Carson GA, *et al.* Valence-band electronic structure of Co_3O_4 epitaxy on CoO(100). Phys Rev B, 1999, 59: 4791–4798
47 Jiménez VM, Fernández A, Espinós JP, *et al.* The state of the oxygen at the surface of polycrystalline cobalt oxide. J Electron Spectr Related Phenomena, 1995, 71: 61–71
48 Zhang HT, Chen XH. Controlled synthesis and anomalous magnetic properties of relatively monodisperse CoO nanocrystals. Nanotechnology, 2005, 16: 2288–2294
49 Carson GA, Nassir MH, Langell MA. Epitaxial growth of Co_3O_4 on CoO(100). J Vacuum Sci Tech A-Vacuum Surfs Films, 1996, 14: 1637–1642
50 Novosad V, Guslienko KY, Shima H, *et al.* Effect of interdot magnetostatic interaction on magnetization reversal in circular dot arrays. Phys Rev B, 2002, 65: 060402
51 Novosad V, Grimsditch M, Darrouzet J, *et al.* Shape effect on magnetization reversal in chains of interacting ferromagnetic elements. Appl Phys Lett, 2003, 82: 3716–3718

Acknowledgements This work was financially supported by the National Key R&D Program of China (2017YFA0206301 and 2016YFA0200102), the National Natural Science Foundation of China (51631001, 51590882, 51672010 and 81421004), and Beijing Natural Science Foundation (L172008).

Author contributions Qiao S performed the experiments; Qiao S and Yang Z analyzed the data and wrote the draft of manuscript; Xu J and Wang X provided some additional suggestions and comments on analyzing the data and the manuscript; Hou Y and Yang J proposed the project and revised the manuscript. All authors contributed to the general discussion and checked the manuscript.

Conflict of interest The authors declare no conflict of interest.

Supplementary information Supporting data are available in the online version of the paper.

Shuang Qiao received her bachelor's degree from University of Science and Technology Beijing in 2015. Currently, she is a master candidate at Peking University. Her current research interest focuses on the synthesis and design of functional magnetic nanomaterials.

Yanglong Hou received his PhD in materials science from Harbin Institute of Technology (China) in 2000. After a short postdoctoral training at Peking University, he worked at the University of Tokyo from 2002 to 2005 as a JSPS foreign special researcher and also at Brown University from 2005 to 2007 as a postdoctoral researcher. He joined Peking University in 2007, and now is a Professor of Materials Science. His research interests include the design and chemical synthesis of functional nanoparticles and graphene, and their biomedical and energy related applications.

Fe_3O_4纳米颗粒修饰的Co纳米棒化学制备、结构及磁学性能研究

乔双[1], 杨子煜[1], 徐俊杰[1], 王晓白[1], 杨金波[2], 侯仰龙[1*]

摘要 各向异性的磁性异质纳米材料因其各组分之间的相互作用, 可获得不同于单一组分的增强性能、甚至出现新的功能特性. 本文通过一种简单的高温液相合成方法, 制备了具备硬磁性能的一维Co-Fe_3O_4异质纳米复合结构. 研究表明, 在此异质结的生长过程中, 铁前驱体是先受热分解并单独形核, 之后, 再通过高温反应在密排六方晶体结构(hcp)Co纳米棒表面进行生长, 有别于常规的晶种-形核生长模式. 另外, Co纳米棒表面负载的Fe_3O_4纳米颗粒的密度可通过反应过程中铁前驱体的添加量进行控制, 进而对其磁学性能如矫顽力(H_c)和饱和磁化强度(M_s)等进行调控. 通过此过程获得的Co-Fe_3O_4异质纳米复合材料表现为硬磁性能, M_s值最高可达128.3 emu g^{-1}, H_c值最高可达2.5 kOe, 较好地保持了原始Co纳米棒的磁各向异性.

